structures eventually become the flame tip which is seen to burn out in a quasiperiodic fashion. Thus, the instantaneous flame length does not vary in a purely random fashion but is a consequence of the organized motion in the flow. These images provide some of the clearest evidence to date to link the underlying organized motion and the resulting flame tip oscillation. Reference 12 also shows that the period of the flame tip oscillation scales properly with the local large-scale variables. Thus, while organization in the near-field is well-established,[13] images such as the ones shown in Fig. 3, begin to demonstrate the combustion implications of the organization that is seen in the jet far-field as illustrated in Fig. 2. Similar findings have been reported in Ref. 14 for liquid jet studies.

Conclusions

The rendering of image sequences used here is of great value in finding temporal correlations in data sequences, as it provides an integrated, global view of the time evolution as opposed to the single instant views produced by a movie loop. By first examining the development of a pulsed low Reynolds number jet, one is able to make the connection between the conventional movie sequence and the new rendered images. Volume renderings of images of a very high Reynolds number jet and a turbulent diffusion flame clearly illustrate organized motions that are more difficult to discern in direct movie projections. The method, we believe, should be equally beneficial when applied to movie sequences of other flows of scientific and technological interest. Although not shown here, the method appears equally applicable to computational results.

Acknowledgment

This research was sponsored by the Air Force Office of Scientific Research, Aerospace Sciences Directorate.

References

[1]Settles, G. S., "Modern Developments in Flow Visualization," *AIAA Journal*, Vol. 24, Aug. 1986, pp. 1313–1323.

[2]Gad-el-Hak, M., "Visualization Techniques for Unsteady Flows: An Overview," *Journal of Fluids Engineering*, Vol. 110, Sept. 1988, pp. 231–243.

[3]Miles, R. B., and Nosenchuck, D.M., "Three Dimensional Quantitative Flow Diagnostics," *Lecture Notes in Engineering 45, Advances in Fluid Mechanics Measurement*, edited by M. Gad-el-Hak, Springer-Verlag, Berlin Heidelberg, 1989, pp. 33–107.

[4]Jimenez, J., Cogollos, M., Bernal, L. P., "A Perspective View of the Plane Mixing Layer," *Journal of Fluid Mechanics*, Vol. 152, 1985, pp. 125–143.

[5]Agui, J.C., and Hesselink, L., "Flow Visualization and Numerical Analysis of a Coflowing Jet: A Three Dimensional Approach," *Journal of Fluid Mechanics*, Vol. 191, 1988, pp. 19–45.

[6]Drebin, R. A., Carpenter, L., and Hanrahan, P., "Volume Rendering," *Computer Graphics*, Vol. 22, No. 4, Aug. 1988, pp. 65–74.

[7]van Cruyningen, I., Lozano, A., and Hanson, R. K., "Volume Rendering of Multidimensional Fluid Flow Images," *SIGGRAPH Video Reviews #44 - Volume Visualization,* and *SIGGRAPH Video Reviews #42-43 - Visualization in Scientific Computing*, edited by T. S. DeFanti, Association for Computing Machinery: Special Interest Group on Computer Graphics, New York, 1989.

[8]van Cruyningen, I., Lozano, A., and Hanson, R. K., "Computer Rendering of Planar Fluorescence Flowfield Images," AIAA Paper 90-0499, Jan. 1989.

[9]Mungal, M. G., and Hollingsworth, D. K., "Organized Motion in a Very High Reynolds Number Jet," *Physics of Fluids A*, Vol. 1, No. 10, 1989, pp. 1615–1623.

[10]Mungal, M. G., Lozano, A., van Cruyningen, I., "Large-Scale Dynamics in High Reynolds Number Jets and Jet Flames,"*Experiments in Fluids, A* (submitted for publication).

[11]Dimotakis, P. E., Miake-Lye, R. C. and Papantoniou, D. A., "Structure and Dynamics of Round Turbulent Jets," *Physics of Fluids*, Vol. 26, No. 11, Nov. 1983, pp. 3185–3192.

[12]Mungal, M.G., Karasso, P. S., and Lozano, A., "The Visible Structure of Turbulent Jet Diffusion Flames: Large-Scale Organization and Flame Tip Oscillation," *Combustion Science and Technology* (submitted for publication).

[13]Chen, L. D., and Roquemore, W. M., "Visualization of Jet Flames," *Combustion and Flame*, Vol. 66, 1986, pp. 81–86.

[14]Dahm, W. J. A., and Dimotakis, P. E., "Measurements of Entrainment and Mixing in Turbulent Jets," *AIAA Journal*, Vol. 25, Sept. 1987, pp. 1216–1223.

Effect of Fiber Modulus Variations on Stress Concentration in Hybrid Composites

J. N. Rossettos* and K. Sakkas†
Northeastern University, Boston, Massachusetts 02115

Introduction

INTEREST in hybrid composites, where more than one type of fiber material is contained in a common matrix, has been prompted by their ability to provide a balance between stiffness and strength. Also, as indicated in Ref. 1, a hybrid effect can be realized, where the higher-modulus fibers have a larger failure strain than when they exist alone in a nonhybrid composite. Fukuda and Chou[1] use shear lag theory[2] to study the stress concentration near broken fibers in hybrid composite sheets. They introduce the parameter R, which is the ratio of the axial stiffness of the low modulus (*LM*) to high modulus (*HM*) fibers, and gives results for $R = 1/3$, a value typical of carbon/glass hybrids.

The present Note gives results for a full range of values of R, for both two-dimensional (sheet) and three-dimensional configurations. As will be seen, the stress concentration drops for *HM* fibers while it rises for the *LM* fibers as R ranges from 1 to 0.2. Direct solution of a matrix system of differential equations using eigenvector expansions provides a convenient means of analysis. The results reduce to those of Fukuda and Chou[1] for $R = 1/3$ and to those of Hedgepeth[2,3] when $R = 1$.

Analysis

In the lamina analysis, we consider a finite-width sheet consisting of $2q + 1$ fibers parallel to the x axis or load direction. The center fiber is the zeroth, and the fibers above it are numbered so that n equals 1 to q. Below it, they are numbered -1 to $-q$. There is an alternating arrangement of HM and LM fibers, where one or more fibers are broken in a continuous manner at $x = 0$. The axial load and displacement in the nth fiber are denoted by $p_n(x)$ and $u_n(x)$. In what follows, asterisks will also denote quantities related to *LM* fibers. Force equilibrium is based on the well-known shear lag model,[2,3] where fibers take the axial load and the matrix is in pure shear and involves a force balance between the varying fiber load, dp_n/dx, and the shear in the matrix on either side of the fiber. For instance, the shear force per unit length between the nth and $n + 1$th fiber, where the nth fiber is *HM*, is $Gh(u^*_{n+1} - u_n)/d$. It is $Gh(u_n - u^*_{n-1})/d$ between the nth and $n - 1$th fiber; d is the distance between fibers and h is sheet thickness. Equilibrium equations are derived as in Ref. 2 and are given for *HM* and *LM* fibers, respectively, as

$$EA\frac{d^2u_n}{dx^2} + \left(\frac{Gh}{d}\right)(u^*_n - 2u_n + u^*_{n-1}) = 0 \quad (n = 0,2,4, \ldots)$$

$$E^*A^*\frac{d^2u^*_n}{dx^2} + \left(\frac{Gh}{d}\right)(u_{n+1} - 2u^*_n + u^*_{n-1}) = 0 \quad (n = 1,3, \ldots) \tag{1}$$

Received Feb. 5, 1990; revision received Feb. 14, 1990.

*Professor, Department of Mechanical Engineering.
†Graduate Student, Department of Mechanical Engineering.

where EA and G are the fiber extensional stiffness and matrix shear modulus. In Eqs. (1), $n = 0$ is an *HM* fiber. The equations are easily written so that $n = 0$ is an *LM* fiber instead. The fiber load-displacement relations are

$$p_n = EA\frac{du_n}{dx}, \qquad p_n^* = E^*A^*\frac{du_n^*}{dx} \tag{2}$$

Nondimensional fiber loads P_n and displacements U_n are next defined, where ξ is a dimensionless coordinate in the x direction.

$$(p_n, p_n^*) = p(P_n, P_n^*); \qquad x = \sqrt{\frac{EA\ d}{Gh}}\,\xi$$

$$(u_n, u_n^*) = p\sqrt{\frac{d}{EAGh}}\,(U_n, U_n^*); \qquad R = \frac{E^*A^*}{EA} \tag{3}$$

where p is the *HM* fiber load at infinity. With Eq. (3), Eqs. (1) and (2) become

$$U_n'' + U_{n+1}^* - 2U_n + U_{n-1}^* = 0 \qquad (n = 0,2,4,\ldots)$$

$$RU_n^{*\prime\prime} + U_{n+1} - 2U_n^* + U_{n-1} = 0 \qquad (n = 1,3,5,\ldots) \tag{4}$$

$$P_n = U_n', \qquad P_n^* = RU_n^{*\prime}, \qquad (\ )' = \frac{d(\ )}{d\xi} \tag{5}$$

For edge fibers that are *HM* fibers, we also have

$$U_q'' + U_{q-1}^* - U_q = 0 \qquad (n = q)$$

$$U_{-q}'' + U_{-q+1}^* - U_{-q} = 0 \qquad (n = -q) \tag{6}$$

The $2q + 1$ Equations (4) and (6) are written in matrix form as

$$U'' - LU = 0 \tag{7}$$

where L is banded and U is the vector $[U_q, U_{q-1}^*, U_{q-2}, \ldots, U_{-q}]$ of nondimensional fiber displacements. Appropriate boundary conditions are given by

$$\begin{aligned}
&\text{At}\xi = \infty, \quad P_n = 1, \quad P_n^* = R, \quad U_n = U_n^* \\
&\text{At}\xi = 0, \quad U_n = 0, \quad U_n^* = 0 \quad \text{unbroken fibers} \\
&\text{At}\xi = 0, \quad P_n = 0, \quad P_n^* = 0 \quad \text{broken fibers}
\end{aligned} \tag{8}$$

where a uniform strain state is assumed at infinity. A solution to Eq. (7) is assumed in the form $U = \boldsymbol{R}e^{\lambda\xi}$ where U and $\boldsymbol{R}$ are vectors of order $2q + 1$. The resulting eigenvalue problem, $(L - \lambda^2 I)\boldsymbol{R} = 0$, leads to eigenvalues λ_i^2 and eigenvectors R^i. The solution U can be written by the superposition of eigenvectors[4,5] as the expansion

$$U = \sum_{i=1}^{2q+1} C_i R^i e^{-\lambda\xi} + Up \tag{9}$$

where the $+\lambda_i$ have been discarded and the particular solution, $U_P{}^T = [\xi, \xi, \ldots, \xi]$, is added in Eq. (9) so that $P_n(\infty) = 1$ and $P_n^*(\infty) = \boldsymbol{R}$ are satisfied. The $2q + 1$ boundary conditions (8) are then used to find the constants C_i.

In the three-dimensional formulation, we consider a square array of fibers that are spaced a distance d apart and are aligned in the x direction. In what follows, $u_{n,m}(x)$ denotes the displacement of the (n,m)th fiber with n and m in the plane normal to all fibers as shown in Fig. 1. Since the interactions of the array of fibers are complex in nature, as a first approximation,[3] it assumed that a given fiber is influenced only by its nearest neighbors. According to Fig. 1, then, the equilibrium of an internal *HM* fiber is influenced by the nearest neighboring *LM* fibers. Similarly, an *LM* fiber has *HM* fibers as its

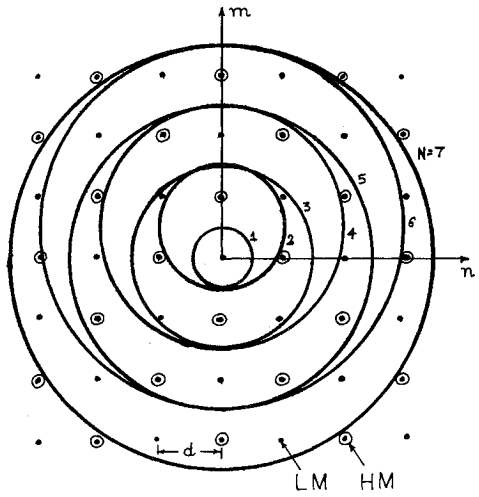

Fig. 1 Three-dimensional fiber geometry, square array.

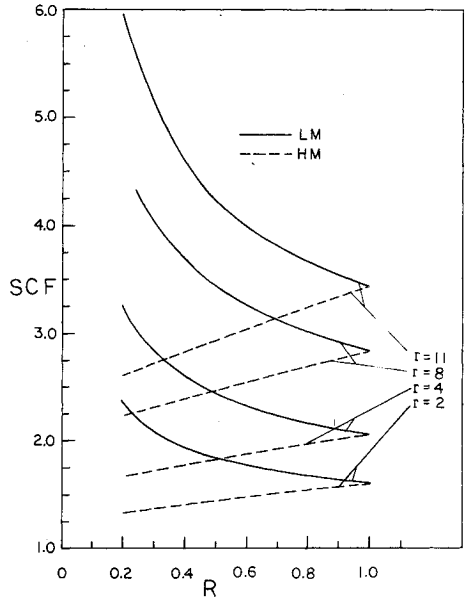

Fig. 2 SCF vs R for *LM* and *HM* fibers for different number of breaks r, two-dimensional model.

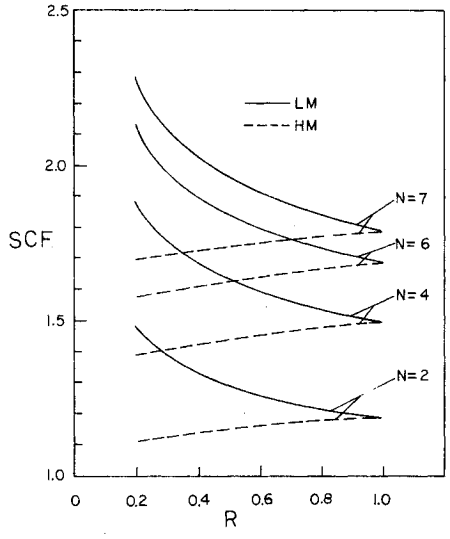

Fig. 3 SCF vs R for *LM* and *HM* fibers for a different number of breaks N on major diameter, three-dimensional model.

nearest neighbors. The equilibrium equations can be derived as in Refs. 3 and 6 and involve a force balance between the fiber in question and the shear force induced by the relative axial displacement of the given fiber and the nearest neighboring fibers via the matrix shear strain. For the *HM* fibers, they are

$$\frac{d^2U_{n,m}}{d\xi^2} + U^*_{n+1,m} + U^*_{n,m+1} + U^*_{n-1,m} + U^*_{n,m-1} - 4U_{n,m} = 0 \tag{10}$$

For *LM* fibers, we get

$$\frac{Rd^2U^*_{n,m}}{d\xi^2} + U_{n+1,m} + U_{n,m+1} + U_{n-1,m} + U_{n,m-1} - 4U^*_{n,m} = 0 \tag{11}$$

Since we deal with finite-width dimensions, additional equations are written[6] for corner and edge fibers. The nondimensional loads are

$$P_{n,m} = U'_{n,m}, \qquad P^*_{n,m} = RU^{*'}_{n,m} \tag{12}$$

and the boundary conditions are the same as in Eqs. (8). For instance, for *HM* fibers, we have

$$P_{n,m}(0) = 0 \ (n,m) \text{ broken}; \ U_{n,m}(0) = 0 \ (n,m) \text{ intact}; \ P_{n,m}(\infty) = 1 \tag{13}$$

The band matrix L in Eq. (7) is now wider, and stress concentration factors (SCF) are calculated in the first unbroken fibers on the major diameter adjacent to the broken fibers. The way in which broken fibers were chosen is the same as in Ref. 3 and is shown in Fig. 1. The number N in Figs. 1 and 3 represents the number of broken fibers on the major diameter and all fibers within a circle of diameter Nd were broken. This approach is motivated for nonhybrids in Ref. 3, where the ratio of the three-dimensional to the two-dimensional SCF is shown to approach the limit $2/\pi$ as N gets very large. This limit is shown to be the same as the corresponding ratio, for the continuous problem, of the three-dimensional SCF as the edge of a disk-shaped void in a three-dimensional body is approached to the two-dimensional SCF as the edge of a crack in a sheet is approached.

Results and Discussion

Results for the stress concentration factor (SCF) in the first unbroken fiber adjacent to a series of fiber breaks are shown in Figs. 2 and 3. In the two-dimensional case, the SCF for an *HM* fiber is equal to the value of P_n in the first unbroken *HM* fiber. For the first unbroken *LM* fiber, it is equal to P^*_n/R. A similar approach is used in the three-dimensional case. Figure 2 plots the SCF against the parameter R for various values of continuous breaks r. In this two-dimensional model, there is a total of 25 fibers. While the SCF increases for the *LM* fibers, it decreases for the *HM* fibers as R goes from 1 to 0.2. This indicates partly how, for smaller values of R, which imply a greater difference in the axial stiffness of the alternating fibers, a greater hybrid effect can be realized. In Fig. 3, the SCF is plotted against R for the three-dimensional model. The number of continuous fiber breaks on the major diameter (see Fig. 1) is given by N, and there is a total of 225 fibers. It is apparent that the SCF for the three-dimensional model is not only less than that for the model, but the two-dimensional model SCF is also more sensitive to R, with greater increases in SCF for *LM* fibers and greater decreases in SCF for *HM* fibers as R goes from 1 to 0.2.

References

[1]Fukuda, H., and Chou, T. W., "Stress Concentrations in a Hybrid Composite Sheet," *ASME Journal of Applied Mechanics*, Vol. 50, Dec. 1983, pp. 845-848.

[2]Hedgepeth, J. M., "Stress Concentrations in Filamentary Structures," NASA TN D-882, 1961.

[3]Hedgepeth, J. M., and Van Dyke, P., "Local Stress Concentrations in Imperfect Filamentary Composite Materials," *Journal of Composite Materials*, Vol. 1, April 1967, pp. 294-309.

[4]Rossettos, J. N., and Shishesaz, M., "Stress Concentration in Fiber Composite Sheets Including Matrix Extension," *ASME Journal of Applied Mechanics*, Vol. 54, Sept. 1987, pp. 722-724.

[5]Strang, G., *Linear Algebra and Its Applications*, Academic, New York, 1980.

[6]Sakkas, K., "Stress Analysis in Hybrid Composites Using the Shear Lag Model," Thesis, Dept. of Mechanical Engineering, Northeastern Univ., Boston, MA, 1986.

Differentia' Equation Based Method for Accurate Modal Approximations

Jocelyn I. Pritchard* and Howard M. Adelman†
Langley Research Center, Hampton, Virginia 23665

Introduction

IT is highly desirable in optimization to be able to calculate the effect of design variable changes without having to perform a full analysis for each design iteration. This need has led to an increased interest in accurate and efficient approximation techniques. Many optimization procedures use first-order Taylor series approximations of the objective function and constraints for this purpose.[1] Taylor series and other approximations are also used outside of optimization for quick assessments of the effect of design changes.[2-9] In this paper, an efficient method is described that significantly extends the range of applicability of approximations beyond the range of the linear Taylor series approach. The key to the new approach is to recognize that the formulas for the sensitivity derivatives of system behavior variables can be interpreted as differential equations that may be solved to obtain closed form exponential approximations. Herein, these approximations will be referred to as the Differential Equation Based (DEB) approximations.

Basis of DEB Method

The DEB method is exemplified by investigating the sensitivity equations for eigenvalues and eigenvectors. First, the method will be developed for the approximation of vibration frequencies, and then mode shapes.

Approximation of Frequencies

As given in Ref. 10, the equation for the derivative of the vibration eigenvalue ω^2 with respect to a design variable, v is

$$\frac{d\omega^2}{dv} = b - a\omega^2 \tag{1}$$

where

$$a = \Phi^T \frac{dM}{dv} \Phi \qquad b = \Phi^T \frac{dK}{dv} \Phi \tag{2}$$

Received Jan. 19, 1990; revision received April 6, 1990; accepted for publication April 26, 1990.

*Research Engineer, Interdisciplinary Research Office, U.S. Army Aerostructures Directorate.

†Deputy Head, Interdisciplinary Research Office, NASA. Member AIAA.